

Article

# From Initial Hit to Crystal Optimization with Microseeding of Human Carbonic Anhydrase IX—A Case Study for Neutron Protein Crystallography

Katarina Koruza <sup>1,\*</sup> , Bénédicte Lafumat <sup>1</sup>, Maria Nyblom <sup>1</sup>, Wolfgang Knecht <sup>1</sup> and Zoë Fisher <sup>1,2,\*</sup>

<sup>1</sup> Department of Biology and Lund Protein Production Platform, Lund University, Sölvegatan 35, 22362 Lund, Sweden; benedicte.lafumat@gmail.com (B.L.); maria.gourdon@biol.lu.se (M.N.); wolfgang.knecht@biol.lu.se (W.K.)

<sup>2</sup> Scientific Activities Division, European Spallation Source ERIC, Box 176, 22100 Lund, Sweden

\* Correspondence: katarina.koruza@biol.lu.se (K.K.); zoe.fisher@esss.se (Z.F.)

Received: 22 October 2018; Accepted: 17 November 2018; Published: 20 November 2018



**Abstract:** Human carbonic anhydrase IX (CA IX) is a multi-domain membrane protein that is therefore difficult to express or crystallize. To prepare crystals that are suitable for neutron studies, we are using only the catalytic domain of CA IX with six surface mutations, named surface variant (SV). The crystallization of CA IX SV, and also partly deuterated CA IX SV, was enabled by the use of microseed matrix screening (MMS). Only three drops with crystals were obtained after initial sparse matrix screening, and these were used as seeds in subsequent crystallization trials. Application of MMS, commercial screens, and refinement resulted in consistent crystallization and diffraction-quality crystals. The crystallization protocols and strategies that resulted in consistent crystallization are presented. These results demonstrate not only the use of MMS in the growth of large single crystals for neutron studies with defined conditions, but also that MMS enabled re-screening to find new conditions and consistent crystallization success.

**Keywords:** crystallization; microseed matrix screening; seeding; optimization; human carbonic anhydrase IX; neutron protein crystallography

## 1. Introduction

Protein crystallization is based on creating a supersaturated solution of a macromolecule with the addition of precipitants (neutral salts, high molecular weight polymers, organic solvents, polyalcohols) and by manipulation of crystallization conditions, including pH, incubation temperature, increased ionic strength, alteration of the dielectric constant of the medium, volume exclusion by polymers, and chemical/biochemical modification of proteins. Different approaches have been developed to promote crystallization, and among the most widely used are sitting or hanging drop vapor diffusion, batch, dialysis, and counter-diffusion techniques [1,2].

Growing large crystals for neutron protein crystallography (NPX) presents a major challenge for structural biologists interested in using neutron scattering. Current neutron instruments for NPX are limited in neutron flux and instrument geometry. This imposes limitations on the size of the crystallographic unit cell parameters, asymmetric unit volume, and it requires a very large overall crystal volume compared to what is sufficient for X-ray crystallographic studies. The general recommendation is to aim for crystals  $\sim 1 \text{ mm}^3$  in volume with  $\sim 30$  out of 160 examples coming from crystals smaller than this [3,4]. A survey of deposited NPX structures in the Protein Data Bank (PDB)

reveals that most large crystals were grown using vapor diffusion. A drop of protein is mixed with precipitant and equilibrated against the reservoir in a sealed environment. In the sitting drop format it can be scaled up to almost any volume and has been reported to be successful in 100–1000  $\mu\text{L}$  drops [5–7]. Batch crystallization has also been used, and here the protein is mixed with precipitant and optionally covered with a layer of oil. In batch, the supersaturation point is reached at the moment of drop preparation, meaning the process does not rely on evaporation [8]. In both techniques, it is challenging to control nucleation and subsequent crystal growth in a consistent and repeatable way.

Seeding is a very powerful strategy, as it allows optimization of crystal growth conditions independently from conditions needed for initial nucleation. Examples in the literature show that seeding in its variations can increase the number of crystallization hits and can significantly shorten the crystallization time [9–11]. It is also possible to incorporate seeding into any crystallization set-up. Seeding is a technique where crystals are crushed in mother liquor or reservoir solution and diluted to create a seed stock that is added to crystallization solutions to aid with nucleation [12,13]. As illustrated in Figure 1, spontaneous nucleation cannot occur in an undersaturated solution, below the solubility line; therefore, seeds introduced in this phase dissolve. Spontaneous homogeneous nucleation occurs in the supersaturation zone, but it can be a long process that takes several months. The supersaturation is low and suitable for crystal growth in the metastable zone, but here nucleation does not occur spontaneously. This zone is ideal for seeding and crystal growth, and seeding can remarkably speed up the crystallization trajectory and provide more consistent control and results [10,11].

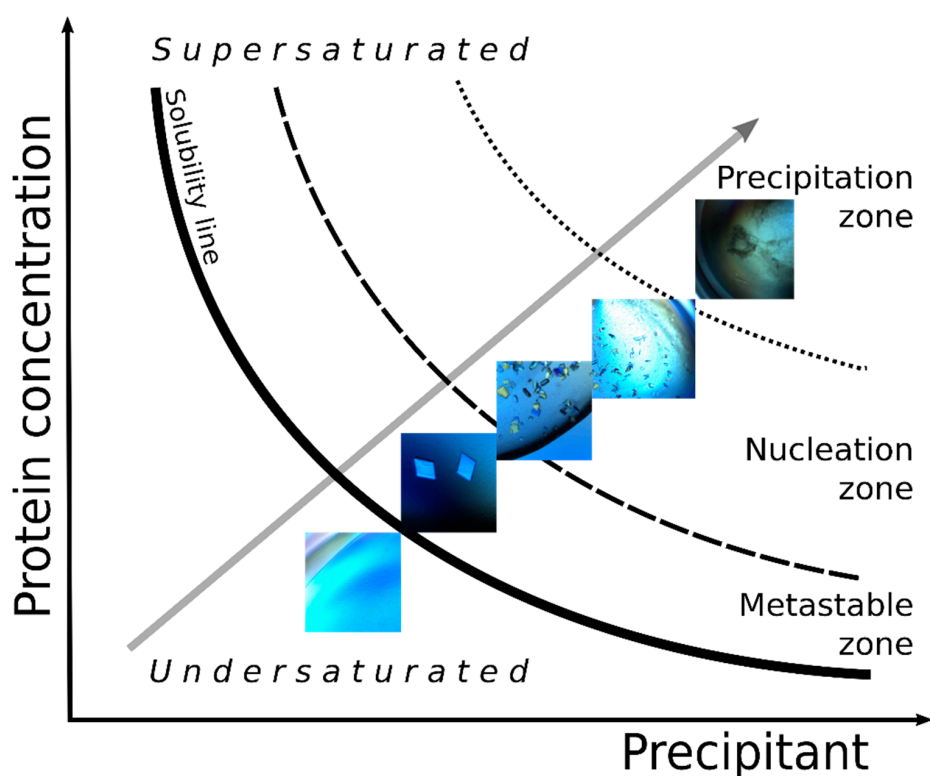


**Figure 1.** A schematic representation of a phase diagram showing the solubility of a protein in solution as a function of the concentration of the precipitant. The grey arrow illustrates the estimated path of crystallization. The path leads from the undersaturated zone below the solubility curve, where no crystals can grow, to the precipitation zone, where supersaturation is too high and protein precipitates without forming crystals. Below the precipitation zone is the nucleation zone, where the supersaturation is high and nucleation is observed, but the crystal growth is slow. In the metastable zone, the nucleation does not occur spontaneously, but the supersaturation is low and suitable for crystal growth [14].

In the nucleation and precipitation zone where spontaneous nucleation occurs, seeding often results in excessive (over)nucleation and can result in the formation of showers of microcrystals or amorphous precipitate [14]. Additionally, the size and number of crystals can be manipulated by systematically using a dilution series of seed stock until an ideal amount of seedstock for a given batch can be identified [15]. This technique can not only help to grow crystals where none grew before, but it can also generate better-diffracting crystals, since crystals are more likely to grow in the metastable zone [14].

Our work is focused on NPX, and for that we need optimized methods to reliably grow large crystals from large volume drops (typically >100  $\mu\text{L}$ ). This is due to the inherent low flux of neutron sources, and crystals have to be 2–3 orders of magnitude larger in volume than what is typical for X-ray crystallography (e.g.,  $\sim 1$  vs.  $\sim 0.01$   $\text{mm}^3$ ). Neutrons are sensitive to H atoms and to its isotope, deuterium (D), whose scattering lengths differ in both magnitude and phase [16]. Partial (including H/D exchange) or full (per)deuteration of proteins presents its own challenges, but it reduces the incoherent scattering background from H, significantly increases the signal-to-noise ratio of the diffraction data, and also makes it possible to use up to an order of magnitude smaller crystals [3,17]. In addition to the requirement of having large, deuterated protein crystals for NPX, there are also limitations to the size of the unit cell that current neutron macromolecular beamlines can resolve. Instruments have different design features that enable some to resolve unit cell parameters of 100–150  $\text{\AA}$  on edge (IMAGINE, LADI-III, BioDIFF, iBIX), while MaNDi is designed to resolve unit cells up to 300  $\text{\AA}$  on edge [4,18]. This limitation remains a challenge, and while a large unit cell can be overcome by having a large crystal, there are very few examples of neutron structures determined from crystals with unit cells over 150  $\text{\AA}$  on any edge. Unit cell parameters are then an important consideration when pursuing neutron studies of a given system. Just as a relatively large unit cell can be overcome by having a large crystal, the converse is also true, in that it becomes more feasible to collect neutron data from a much smaller crystal if the unit cell is also small [3,16,19].

In the work presented here, we worked with both hydrogenous and deuterated versions of the same protein. As large crystals can take a long time to grow, it is necessary to use set-ups that are stable for long incubation and equilibration periods. It is desirable to control the thermodynamic and kinetic contribution to the supersaturated state where the protein crystal nucleates, and this can be done by controlling temperature, evaporation rates, and pH, protein, and precipitant concentrations. Automation and systematic screening gives better control of the supersaturation state by having the possibility to screen a large area around crystallization hits. Seeding, in conjunction with large drop volume, provides a way to speed up crystal growth, as well as a way to control the number of crystals in a given drop.

The protein we are working with is human carbonic anhydrase IX (CA IX). CA IX is implicated in cancer metastasis and has emerged as a target for cancer detection, imaging, and treatment [20]. We are using neutrons to obtain details of the enzyme active site with regards to hydrogen bonding, water organization, and ligand binding interactions that will enable rational drug design efforts [16]. However, the native protein is 459 amino acids (UniProtKB-Q16790) with multiple domains, including a membrane spanning domain [20]. There are two reports on the structure of the catalytic domain of native CA IX, but the unit cell and parameters are unsuitable for neutron studies [21,22]. The most recent is from CA IX prepared by expression in yeast, and the space group was H3 with unit cell parameters:  $a = b = 152.7$   $\text{\AA}$ ,  $c = 170.7$   $\text{\AA}$ ;  $\alpha = \beta = 90^\circ$ ,  $\gamma = 120^\circ$  (PDB ID 6fe2) [22]. The first structure that was reported was also for the catalytic domain of CA IX, but produced in insect cells and crystallized in P6<sub>1</sub> with unit cell parameters:  $a = b = 144.2$   $\text{\AA}$ ,  $c = 208.9$   $\text{\AA}$ ;  $\alpha = \beta = 90^\circ$ ,  $\gamma = 120^\circ$  (PDB ID 3iai) [21]. Due to the previously mentioned challenges regarding size and unit cell volumes, we are, therefore, working with a construct composed of residues 140–395 of human CA IX, that also contains six mutations engineered at the surface of the protein (hence called surface variant: CA IX SV). The mutated residues C174S, L180S, A210K, A258K, F259Y, and M360S were designed to make the catalytic domain more soluble, suitable for expression in *E. coli*, and also to be more amenable to crystallization [23].

While surface mutations are introduced away from the highly conserved active site of the enzyme, the catalytic efficiency of the SV enzyme is decreased in comparison with native protein, as described by Mahon et al. [23]. The CA IX SV was previously reported to crystallize in  $P2_12_12_1$  with unit cell parameters  $\sim 100$  Å on edge using 8% PEG 8000, 0.1 M Tris pH 8.5, and as such is more suitable for neutron studies than working with the native protein [21–23]. Despite extensive efforts to reproduce these conditions, we were unable to obtain any crystals. Here we present the details of starting over with nanoliter drops in high-throughput set-ups with commercial screens and going from a single initial hit to optimization for consistent growth of diffraction-quality single crystals. A crystallization strategy of microseed matrix screening (MMS), as described by Ireton and Stoddard, was used [24]. In this method, crystal seeds or nuclei from one crystallization condition are added systematically to a matrix of various conditions to screen for new conditions that promote crystal growth [24].

## 2. Materials and Methods

### 2.1. Protein Preparation

The catalytic domain of human CA IX was expressed in *E. coli* BL21(DE3) under hydrogenous and deuterated conditions according to a protocol described in detail elsewhere [23,25]. In this previous work the focus was to optimize deuteration strategies to produce different levels of D incorporation and to measure biophysical effects on the resulting proteins. To measure how deuteration affects crystallization behavior, we chose a single condition from this work to set-up side-by-side crystallization of H and D versions of the same proteins [25]. The protein was previously engineered to have 6 surface mutations that provide a more soluble and stable enzyme, which we refer to as the CA IX surface variant (CA IX SV) [23]. CA IX SV was purified using para-aminobenzenesulfonamide resin (pAMBS, Sigma-Aldrich, Stockholm, Sweden), followed by size exclusion chromatography (Superdex200 16/600, GE Healthcare, Uppsala, Sweden). The protein elutes in 50 mM Tris pH 8.5, 100 mM NaCl in 2 peaks. Both peaks 1 and 2 were tested for crystallization, and only peak 2 yielded any crystals [25]. Fractions containing peak 2 were pooled and concentrated to 12–17 mg/mL, depending on the preparation batch.

### 2.2. Crystallization

Published crystallization conditions around 8% PEG 8000, 0.1 M Tris pH 8.5 for concentrations of CA IX SV ranging from 10.8 mg/mL to 17.5 mg/mL, were used to set up crystallization screens at different temperatures (4, 18 °C, ambient) in vapor diffusion experiments [23]. To find new conditions, high-throughput screening was performed with a Mosquito (TTP Labtech, Melbourn, UK) crystallization robot for droplets with a final volume of 300 nL (protein:precipitant ratio of 1:1, reservoir volume 40 µL), or with an Oryx8 (Douglas instruments, Hungerford, UK) in vapor diffusion, or under-oil microbatch drops (protein:precipitant:seeds ratio of 3:2:1, final drop volume 0.6 µL, reservoir volume 40 µL). Four commercial crystallization screens were used in the initial rounds: JCSG+ (Molecular Dimensions, Newmarket, UK), Morpheus (Molecular Dimensions, Newmarket, UK), PurePEGs (Anatrace, Maumee, OH, USA), and TOP96 (Anatrace, Maumee, OH, USA). MRC crystallization plates from Molecular Dimensions were used for sitting drop format, while for the microbatch under-oil set-up we used hydrophilic plasma treated plates (Douglas Instruments, Hungerford, UK). Oils used were paraffin oil, silicon oil, and Al's oil (1:1 mix of paraffin and silicon oil). In manual set-ups for larger hanging and sitting drops (protein:precipitant:seeds ratio of 3:2:1, final drop volume 3–24 µL, reservoir volume 1 mL), 24-well Linbro plates (Hampton Research, Aliso Viejo, CA, USA) were used. Crystallization drops were always mixed in order, precipitant–protein–seeds, using freshly prepared buffers and PEG solutions (*w/v*).

Seed stocks for microseeding experiments were prepared according to Seed Bead™ Kit instructions (<https://www.hamptonresearch.com>; collected 2018-10-06) using reservoir solution from the crystallization condition. For seeding optimization the stock was tested in a dilution series. In

between crystallization experiments the seed stocks were stored in a  $-80\text{ }^{\circ}\text{C}$  freezer. Cross-seeding was attempted with human CA isoform II crystal seeds [26]. Seeding was used for both manual and automated experiments with Oryx8 (Douglas instruments). All crystallization plates were incubated at  $20\text{ }^{\circ}\text{C}$  and inspected under polarizing light microscope, or with the Minstrel HT UV imaging system (Rigaku). Hydrogenous and deuterated proteins were crystallized using the same hydrogenous precipitant solutions with no adaptation. Table 1 and Figure 2 show summaries of all conditions eventually identified. Crystals were visually inspected and evaluated based on relative size and quality (single, not aggregated, clean edges, no or little precipitation in the drops).

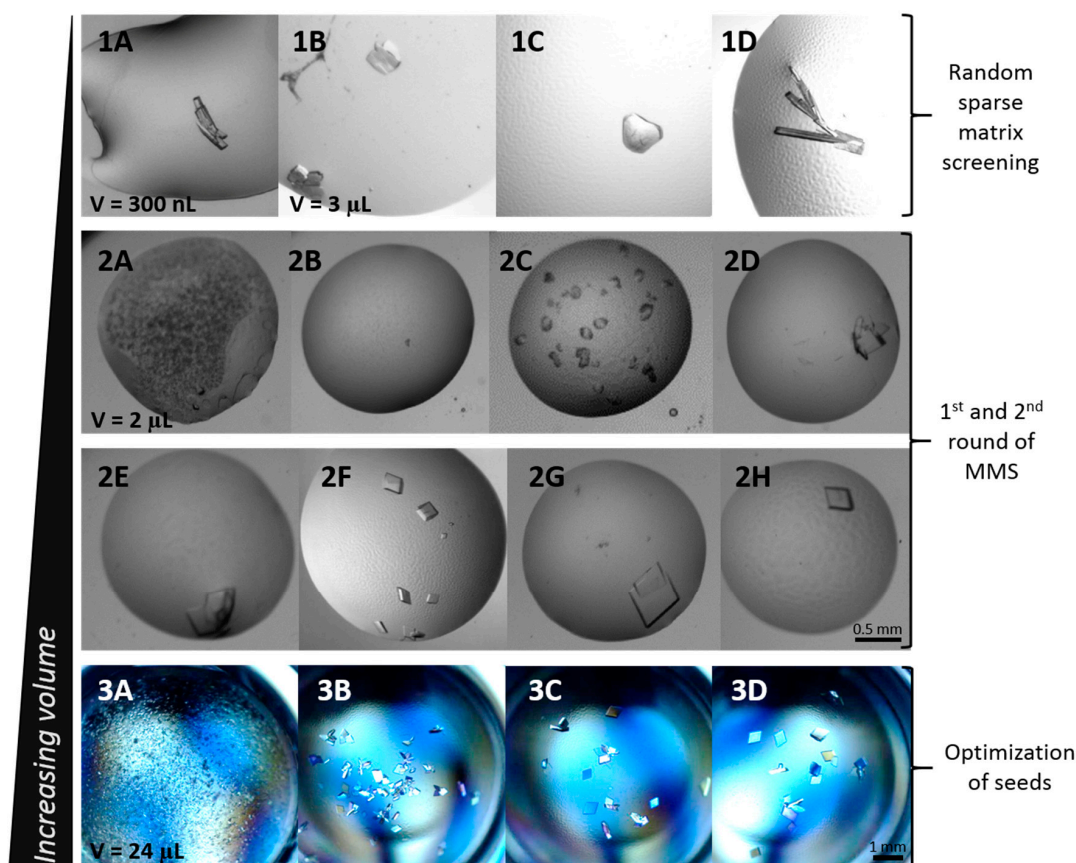


**Figure 2.** Crystallization of CA IX SV from initial hit to optimized crystals used for diffraction. Drop volumes are indicated per row. The initial screening hit appeared in (1A) 20% PEG 3350, 0.2 M ammonium formate (JCSG+). Systematic alternation of the initial conditions was performed in hanging drop set-up. Observed crystals were used for two seed stocks. The first seed stock was prepared from (1B) 0.1 M Tris pH 7.5, 22% PEG 3350, 0.2 M NaCl, and the second seed stock was from a mixture of (1C) 0.1 M Tris pH 7.0, 20% PEG 4000, 0.2 NaCl and (1D) 0.1 M Tris pH 7.5, 20% PEG 6000, 0.2 M NaCl. The two seed stocks were diluted  $10\times$  and seeded into JCSG+, Morpheus, PurePEGs, and TOP96 screens for a second round of MMS. The two rounds of MMS resulted in numerous new conditions (2A–H): (2A) 0.1 M sodium cacodylate pH 6.5, 1 M sodium citrate, (2B) 0.1 M ammonium citrate pH 5, 22.5% PurePEGs Cocktail, 0.3 M cesium chloride, (2C) 0.1 M Tris pH 5.5, 25% PEG 3350, 0.2 M magnesium chloride, (2D) 0.1 M HEPES pH 7.5, 25% PEG 3350, 0.2 M ammonium acetate, (2E) 0.1 M HEPES pH 7.5, 20% PEG 4000, 10% 2-propanol, (2F) 0.1 M Tris pH 8.5, 30% PEG 4000, 0.2 M sodium acetate, (2G) 0.1 M Tris pH 8.5, 25% PEG 3350 and (2H) 0.1 M HEPES pH 7.5, 25% PEG 3350. The crystallization condition that was used to prepare crystals of the H/D exchanged and deuterated (D/D) CA IX SV protein corresponds to (2F). When scaling up the drop size, seed concentration had to be optimized. Seeds stocks used were diluted  $10\times$  (3A), diluted  $100\times$  (3B),  $1000\times$  (3C), and  $10,000\times$  (3D) in  $24\text{ }\mu\text{L}$  drops.

**Table 1.** Summary of crystallization conditions that yielded crystals.

Precipitant	Buffer	pH	Additive/Extra	Crystallization Set-Up	Correlation to Figure 2
20% PEG 3350	None	n/a	0.2 M Ammonium Formate	Hanging drop	1A <sup>1</sup>
20–24% PEG 3350	0.1 M Tris	7.0	None	Sitting drop	n/a
25% PEG 3350	0.1 M HEPES	7.5	None	Sitting drop	2H
20–24% PEG 3350	0.1 M Tris	8.0	None	Sitting drop	n/a
25% PEG 3350	0.1 M Tris	8.5	None	Sitting drop	2G
25% PEG 3350	0.1 M Tris	5.5	0.2 M Magnesium Chloride	Sitting drop	2C
20–26% PEG 3350	0.1 M Tris	7.0	4–10% 2-propanol	Sitting drop	n/a
25% PEG 3350	0.1 M HEPES	7.5	0.2 M Ammonium Acetate	Sitting drop	2D
22% PEG 3350	0.1 M Tris	7.5	0.2 M Sodium Chloride	Hanging drop, microbatch	1B <sup>1</sup>
20–26% PEG 3350	0.1 M Tris	8.0	4–10% 2-propanol	Sitting drop	n/a
18–22% PEG 4000	0.1 M Tris	7.0	None	Sitting drop	n/a
18–22% PEG 4000	0.1 M Tris	7.0	0.2 M Sodium Chloride	Hanging drop, microbatch	1C <sup>1</sup>
20% PEG 4000	0.1 M HEPES	7.5	10% 2-propanol	Sitting drop	2E
22–26% PEG 4000	0.1 M Tris	8.0	10% 2-propanol	Sitting drop	n/a
30% PEG 4000	0.1 M Tris	8.5	0.2 M Sodium Acetate	Sitting drop, microbatch	2F, 3A–D
18–22% PEG 6000	0.1 M Tris	7.5	None	Sitting drop	n/a
18–22% PEG 6000	0.1 M Tris	7.5	0.2 M Sodium Chloride	Hanging drop	1D <sup>1</sup>
22.5% PurePEGs Cocktail	0.1 M Citric Acid 0.1 M	3.5	0.3 M Sodium Formate	Sitting drop	n/a
22.5% PurePEGs Cocktail	Ammonium Citrate	5.0	0.3 M Cesium Chloride	Sitting drop	2B
22.5% PurePEGs Cocktail	0.1 M Sodium Cacodylate	6.5	0.3 M Magnesium Chloride	Sitting drop	2A
1.0 M Sodium Citrate	0.1 M Sodium Cacodylate	6.5	None	Sitting drop	n/a

<sup>1</sup> These are the only crystallization conditions where spontaneous nucleation occurred.

### 2.3. Deuterium Labeling and X-ray Analysis

Crystals of hydrogenous CA IX SV were grown under hydrogenous conditions and were kept in hydrogenous buffers during the experiment (H/H CA IX SV). In parallel, crystals of H/H CA IX SV were subjected to H/D exchange by exchanging the well solution for deuterated solutions and resealed for several weeks to allow labile hydrogen atoms to exchange for deuterium (H/D CA IX SV). Deuterated CA IX SV was crystallized with hydrogenous buffers and then later exchanged to regain lost D atoms in labile positions (D/D CA IX SV). Crystals were cryoprotected by quick dipping in reservoir solution supplemented with glycerol (20% *v/v* final concentration) and flash frozen in liquid nitrogen. Crystals were tested for diffraction at the BioMAX beamline at the MAX IV laboratory. Diffraction data statistics are shown in Table 2. Structure refinement is ongoing.

**Table 2.** X-ray diffraction data set statistics for CA IX SV.

	H/H	H/D	D/D
Wavelength (Å)	0.979	0.979	0.979
Beamline, source	BM-30 (FIP), ESRF	BioMAX, MAX IV laboratory	BioMAX, MAX IV laboratory
Space group, unit cell	P2 <sub>1</sub> ; a = 44.3, b = 65.1, c = 46.7; β = 115.1	P2 <sub>1</sub> ; a = 44.5, b = 65.4, c = 46.7; β = 115.1	P2 <sub>1</sub> ; a = 44.4, b = 65.1, c = 46.6; β = 114.7
Resolution range (Å)	50.0–1.77 (1.88–1.77)	40.0–1.39 (1.42–1.39)	40.0–1.49 (1.51–1.49)
Total No. of reflections	63,296 (9199)	327,912 (15,926)	265,165 (13,184)
No. of unique reflections	22,187 (3463)	48,352 (2406)	39,461 (1948)
Redundancy	2.8 (2.6)	6.8 (6.6)	6.7 (6.8)
Completeness (%)	95.1 (92.9)	99.8 (99.1)	99.9 (99.3)
$\langle I/\sigma(I) \rangle$	10.5 (2.2)	19.9 (2.2)	14.3 (2.2)
R <sub>merge</sub> <sup>†</sup> (%)	6.3 (48.6)	3.6 (78.1)	6.0 (78.1)

$$^{\dagger} R_{\text{merge}} = (\sum |I - \langle I \rangle| / \sum \langle I \rangle) \times 100.$$

### 3. Results & Discussion

#### 3.1. Initial Screening

Narrow screens for CA IX SV, ranging from 6 to 10% PEG 8000 (0.1 M Tris pH 8.5) around published crystallization conditions (8% PEG 8000, 0.1 M Tris pH 8.5), were used to set up hanging drops at different temperatures (4, 12, 18 °C, ambient) [23]. Despite extensive efforts to recreate the reported crystallizations, we had no success. Protein expression and purification was attempted exactly as previously published but did not yield any crystals [23]. The CA IX SV construct shares 36% of its sequence identity with CA II; however, an attempt to do cross-seeding with human CA isoform II crystals did not result in any hits. In a recent study, Abuhammad et al. reported successful crystallization, increased number of hits, and shorter crystallization times when seeds from protein crystals with sequence identities as low as 24% were used [9]. The search for new conditions started with random sparse matrix screening using two commercial screens, JCSG+ and Morpheus (both from Molecular Dimensions). Small drops were prepared with a Mosquito (TTP Labtech) crystallization robot in a sitting drop format using 96-well MRC crystallization plates. The first and only crystallization hit was from JCSG+ (20% PEG 3350, 0.2 M ammonium formate pH 6.5) and was observed after 30 days (Figure 2(1A)). This hit condition formed the basis of systematic alternation of the initial conditions where 16–24% PEG 3350 (or 4000 or 6000 or 8000) with either 0.2 M NaCl or 0.2 M ammonium formate were included. The pH was also varied in 0.5 unit increments from pH 7.0–9.0. The drops were hanging drop and had a final volume of 3 µL and a protein:precipitant ratio of 1:1. Crystals appeared in three of these drops after ~65 days from PEG 3350, 4000, and 6000 (20–22%) supplemented with 0.2 M NaCl and 0.1 M Tris pH 7.0/7.5 (Figure 2(1B–1D)). There were no spontaneous crystals appearing at the reported higher pH of 8.5 or with PEG 8000 in these initial screens.

#### 3.2. Microseed Matrix Screening (MMS)

The drop shown in Figure 2(1B) was sacrificed for seed stock preparation with its reservoir solution (0.1 M Tris pH 7.5, 22% PEG 3350, 0.2 M NaCl), and this stock was used in the first round of MMS using four commercial screens: JCSG+, Morpheus, PurePEGs, and TOP96. The volume of seeds added to the screens was 0.1 µL. The crystals from Figure 2(1C,1D) were later used to prepare a second seed stock using 0.1 M Tris pH 7.0, 20% PEG 4000, 0.2 NaCl, and were also used as an additive for automated microseeding experiments with the Oryx8 (Douglas instruments). Seeding experiments resulted in the identification of numerous new conditions out of the 384 tested (summarized in Table 1; some shown in Figure 2(2A–2H)).

The expanded hits covered a broad range of PEG sizes (Table 1). PEG 3350 appeared on ten occasions, PEG 4000 on five, PEG 6000 on two, and PurePEGs cocktail on three occasions, and ranged between 18% and 30% (*w/v*). A number of additional additives, including magnesium chloride, sodium acetate, ammonium acetate, and 2-propanol also appeared, and seven hits did not contain any (Table 1; Figure 2(2G)). We also found a non-PEG condition with sodium citrate, but due to the crystal appearance, we did not explore it further (Figure 2(2A)). A broad range of pHs also became accessible from the expanded screen results, with CA IX SV crystallizing between pH 3.5–8.5 (Table 1).

The distribution of the number of crystallizations of all the PEG conditions is shown in Figure 3 as a function of pH, PEG size, PEG concentration, and additives. The highest number of hits appears to group around conditions with pH above 7, in range of 18–26% PEG 3350 or 4000, without additive or with NaCl or isopropanol. We did not observe differences in conditions yielding crystals between batch or vapor diffusion set-ups in the smaller volumes (0.3–15 µL) (Figure 4). The outcome of the automated seeding experiments was firstly a control over consistent nucleation at lower levels of supersaturation. Secondly, the conditions where crystals grew varied from the conditions where crystal nucleation occurred and actually resulted in new hits yielding crystals that had different shapes. In terms of time, optimization without seeds would, for some batches of fresh protein, never yield

crystals, while seeding in small volumes reduced the time to get crystals from weeks or even months to only days.

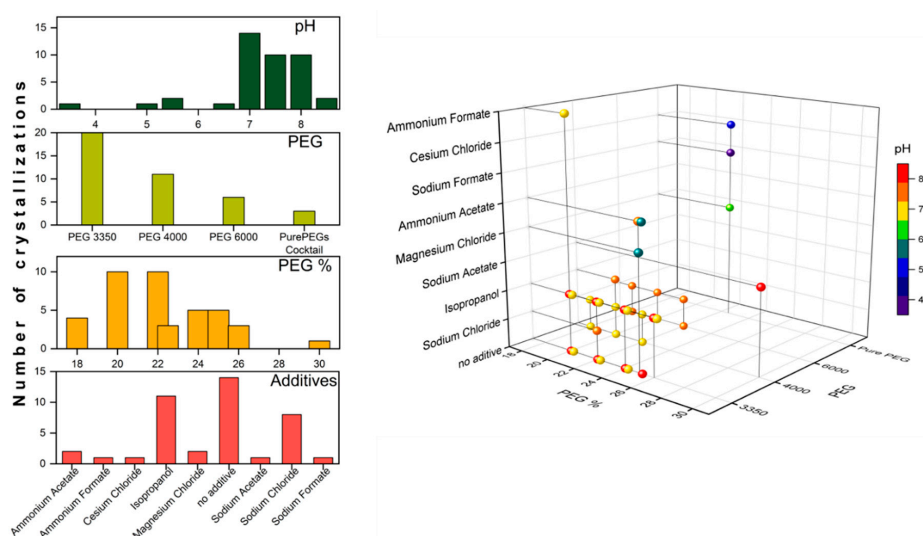


**Figure 3.** Distribution of the number of successful protein crystallizations of all PEG conditions found in systematic screening as a function of pH, size of the PEG, PEG %, and which additives were included. A 3D graph that displays all of the components of the PEG conditions is shown on the right.

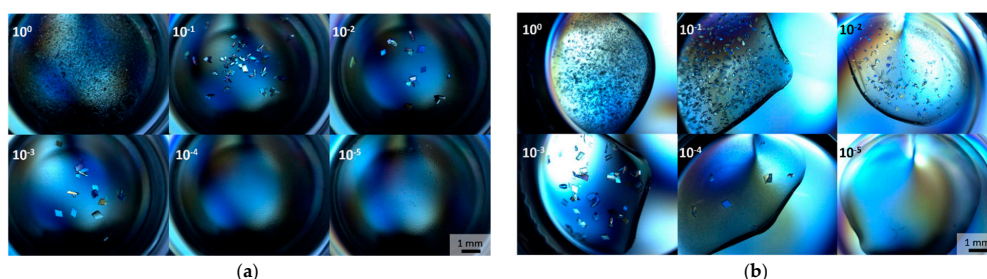


**Figure 4.** The effect of diluting and testing the seed stock solution. Crystallization drops were set up in 0.1 M Tris pH 8.5, 30% PEG 4000, 0.2 M sodium acetate in a ratio of 3:2:1 (protein:precipitant:seeds) in (a) vapor diffusion sitting drop set-up (total drop volume is 24  $\mu$ L) and (b) microbatch with paraffin oil set-up (total drop volume is 15  $\mu$ L).

### 3.3. Optimization with Seed Concentration

The conditions summarized in Table 1 and Figure 2 that resulted in visually the best crystals were scaled up in volumes from 3 to 24  $\mu$ L, initially. Crystal quality was ranked based on being single, having clear edges, and containing no inclusions. The Hampton Research recommended ratio of seed stock to use is 3:2:1 (protein:precipitant:seeds), and while this worked well in smaller drops, when we scaled up to 24  $\mu$ L we observed overnucleation when using 10 $\times$  diluted seed stocks (Figure 2(3A)). The high number of seeds introduced into the crystallization drop resulted in numerous small crystals, but yielded improved results, i.e., fewer and larger crystals per drop (Figure 2(3C,3D)) when prepared in a 1000 $\times$  and 10,000 $\times$  dilution series. The condition that produced the first good crystals selected for X-ray diffraction testing was 22% PEG 3350, 0.2 M NaCl, 0.1 M Tris pH 7.5 (Figure 2(1B)). However, it was later observed that this condition, when using different protein batches, was not consistently successful in giving any crystals, let alone for large crystal growth. After some additional trials, the condition that consistently produced the largest crystals, regardless of the protein batch and length of protein storage, was 30% PEG 4000, 0.2 M sodium acetate, 0.1 M Tris pH 8.5 (Figure 2(2F)).

This condition was successfully used to prepare crystals of the H/D exchanged and deuterated (D/D) CA IX SV protein. Crystals from numerous conditions were selected for X-ray diffraction,

but this condition gave the best diffraction data sets for H/H, H/D, and D/D CA IX SV. X-ray diffraction data collection statistics are shown in Table 2, and the refinement and structures are ongoing and will be reported elsewhere.

Through our MMS approach, we were not only able to gain consistent control over nucleation and crystal growth, we also obtained a new space group ( $P2_1$ ) with smaller unit cell parameters than the previously reported  $P2_12_12_1$ ;  $a = 44.5$ ,  $b = 65.4$ ,  $c = 46.7$  Å,  $\beta = 115.1^\circ$  vs.  $a = 57.9$ ,  $b = 102.7$ ,  $c = 109.0$  Å (Table 2) [23]. The monoclinic space group reported here has a monomer in the asymmetric unit (ASU) compared to a non-crystallographic dimer in the orthorhombic space group. This fortuitous discovery is very beneficial for planned NPX experiments where large crystals with smaller unit cells are required.

### 3.4. Deuterated CA IX SV and Large Volume Crystallization

It has been demonstrated for different proteins, including different human CA proteins, that side-by-side crystallization with the same conditions produced variable outcomes depending on the deuteration level of the protein [25–27]. Initial structural analysis shows that the resulting X-ray crystal structures are unchanged, but the optimal crystallization conditions can be affected and may have to be adjusted for deuterated protein crystal growth.

For neutron protein crystallography we need substantially larger crystals, one to two orders of magnitude larger in volume than what is routinely used for X-ray diffraction. We attempted larger drop set-ups with the best conditions used for X-rays (e.g., Figure 2(2E–2H)); however, scaling up to 50–150  $\mu\text{L}$  with diluted seeds did not reproduce the results from the smaller drops, and conditions had to be re-explored and refined in larger drops. We were finally able to grow a large crystal of H/H CA IX SV from a 150  $\mu\text{L}$  drop using 24% PEG 4000, 10% (*v/v*) 2-propanol, 0.1 M Tris pH 8.0 (Figure 5). We can speculate that, in addition to the chemical parameters (precipitant, pH, and salts), this condition promotes crystallization in large volume by manipulating the dielectric properties of the solution by presence of 2-propanol. All of these factors together successfully created a supersaturated solution and resulted in growth of large single crystals of CA IX SV in nine to 12 months.

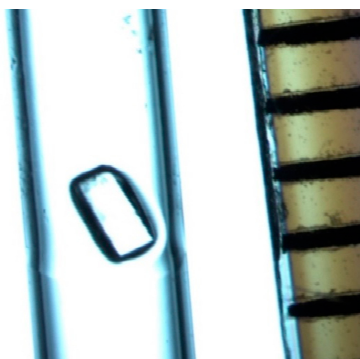


**Figure 5.** CA IX SV crystal mounted in a capillary. Approximate crystal dimensions are  $1.3 \times 0.8 \times 0.8$  mm (volume  $\sim 0.8$  mm<sup>3</sup>), lined ruler visible is graduated in mm increments.

## 4. Conclusions

For this challenging protein, the combination of microseeding, where crystal growth is induced at low levels of supersaturation, and random sparse matrix screening yielded numerous conditions over a broad range of PEGs, additives, and pH. Additionally, the microseeding allowed us to get diffraction quality crystals for different batches of H/H, H/D, and D/D CA IX SV with a limited amount of material and in a reasonable time frame. Conditions that appeared as the result of automated high-throughput screening in small volumes (300 nL) did not scale as expected. Some screening and refining was necessary when volumes were increased >10-fold from the initial hit volume. The amount and size of the PEG varied greatly, from 18–30% PEG and sizes 3350, 4000, and 6000 all gave good

crystals. Throughout our screening efforts, we did not find a condition with PEG larger than 6000. The type of additive did not seem to affect crystal morphology or how fast they appeared in small volumes (0.3–6  $\mu$ L). However, for scaling up the crystallization drop volume beyond 50  $\mu$ L, isopropanol was a better additive than the others. An unexpected bonus coming out of these studies was that we were able to find new conditions that gave us consistent control over crystallization. We prepared well-diffracting crystals in a space group with smaller unit cell parameters than are suitable for neutron diffraction experiments. In short, our work here demonstrates the necessity of broad screening and subsequent continuous optimization while scaling up crystallization volumes as a pre-requisite for preparing CA IX SV crystals suitable for NPX. This approach may be beneficial and generally applicable to other challenging targets, as well, especially where larger crystals are required to enable X-ray or neutron diffraction experiments.

**Author Contributions:** Conceptualization: K.K., W.K. and Z.F.; formal analysis: K.K., B.L., M.N. and Z.F.; investigation: K.K., B.L. and M.N.; methodology: K.K., B.L. and M.N.; supervision: Z.F.; writing—original draft: K.K.; writing review and editing: K.K., M.N., W.K. and Z.F.

**Funding:** This research was partly funded by: Integrated Infrastructure Initiative No. 262348 European Soft Matter Infrastructure, SINE2020. We thank Lund University, the Royal Physiographic Society of Lund, Interreg/MAX4ESSFUN, The Crafoord Foundation No. 20160528, and BioCARE (a strategic research area at Lund University) for financial support.

**Acknowledgments:** The authors would like to thank the MAX IV laboratory (BioMAX) beamline scientists for expert assistance, and the Lund Protein Production Platform (LP3) staff for providing technical support for experiments and for data collection. We would also like to extend sincere thanks to Motoyasu Adachi from the National Institutes for Quantum and Radiological Science and Technology (Tokai, Japan) for useful discussions and advice.

**Conflicts of Interest:** The authors declare no conflict of interest. The funders had no role in the design of the study; in the collection, analyses, or interpretation of data; in the writing of the manuscript, or in the decision to publish the results.

## References

1. Ng, J.D.; Gavira, J.A.; García-Ruiz, J.M. Protein crystallization by capillary counterdiffusion for applied crystallographic structure determination. *J. Struct. Biol.* **2003**, *142*, 218–231. [[CrossRef](#)]
2. McPherson, A.; Gavira, J.A. Introduction to protein crystallization. *Acta Crystallogr. F Struct. Biol. Cryst. Commun.* **2014**, *70*, 2–20. [[CrossRef](#)] [[PubMed](#)]
3. Blakeley, M.P.; Hasnain, S.S.; Antonyuk, S.V. Sub-atomic resolution X-ray crystallography and neutron crystallography: Promise, challenges and potential. *IUCr* **2015**, *2*, 464–474. [[CrossRef](#)] [[PubMed](#)]
4. Meilleur, F.; Coates, L.; Cuneo, M.; Kovalevsky, A.; Myles, D. The neutron macromolecular crystallography instruments at Oak Ridge National Laboratory: Advances, challenges, and opportunities. *Crystals* **2018**, *8*, 388. [[CrossRef](#)]
5. O'Dell, W.B.; Swartz, P.D.; Weiss, K.L.; Meilleur, F. Crystallization of a fungal lytic polysaccharide monoxygenase expressed from glycoengineered *Pichia pastoris* for X-ray and neutron diffraction. *Acta Crystallogr. F Struct. Biol. Cryst. Commun.* **2017**, *73*, 70–78. [[CrossRef](#)] [[PubMed](#)]
6. Ohlin, M.; von Schantz, L.; Schrader, T.E.; Ostermann, A.; Logan, D.T.; Fisher, S.Z. Crystallization, neutron data collection, initial structure refinement and analysis of a xyloglucan heptamer bound to an engineered carbohydrate-binding module from xylanase. *Acta Crystallogr. F Struct. Biol. Cryst.* **2015**, *71*, 1072–1077. [[CrossRef](#)] [[PubMed](#)]
7. Manzoni, F.; Saraboji, K.; Sprenger, J.; Kumar, R.; Noresson, A.-L.; Nilsson, U.J.; Leffler, H.; Fisher, S.Z.; Schrader, T.E.; Ostermann, A.; et al. Perdeuteration, crystallization, data collection and comparison of five neutron diffraction data sets of complexes of human galectin-3C. *Acta Crystallogr. D Struct. Biol.* **2016**, *72*, 1194–1202. [[CrossRef](#)] [[PubMed](#)]
8. Gerlits, O.O.; Coates, L.; Woods, R.J.; Kovalevsky, A. Mannobiose binding induces changes in hydrogen bonding and protonation states of acidic residues in Concanavalin A as revealed by neutron crystallography. *Biochemistry* **2017**, *56*, 4747–4750. [[CrossRef](#)] [[PubMed](#)]

9. Abuhammad, A.; McDonough, M.A.; Brem, J.; Makena, A.; Johnson, S.; Schofield, C.J.; Garman, E.F. “To Cross-Seed or Not To Cross-Seed”: A Pilot Study Using Metallo- $\beta$ -lactamases. *Cryst. Growth Des.* **2017**, *17*, 913–924. [[CrossRef](#)]
10. Obmolova, G.; Malia, T.J.; Teplyakov, A.; Sweet, R.W.; Gilliland, G.L. Protein crystallization with microseed matrix screening: Application to human germline antibody Fabs. *Acta Crystallogr. F Struct. Biol. Cryst.* **2014**, *70*, 1107–1115. [[CrossRef](#)] [[PubMed](#)]
11. D’Arcy, A.; Mac Sweeney, A.; Haber, A. Using natural seeding material to generate nucleation in protein crystallization experiments. *Acta Crystallogr. D Biol. Crystallogr.* **2003**, *59*, 1343–1346. [[CrossRef](#)] [[PubMed](#)]
12. Blakeley, M.P.; Kalb, A.J.; Helliwell, J.R.; Myles, D.A. The 15-K neutron structure of saccharide-free Concanavalin A. *Proc. Natl. Acad. Sci. USA* **2004**, *101*, 16405–16410. [[CrossRef](#)] [[PubMed](#)]
13. Gavira, J.A.; Hernandez-Hernandez, M.A.; Gonzalez-Ramirez, L.A.; Briggs, R.A.; Kolek, S.A.; Shaw Stewart, P.D. combining counter-diffusion and microseeding to increase the success rate in protein crystallization. *Cryst. Growth Des.* **2011**, *11*, 2122–2126. [[CrossRef](#)]
14. Asherie, N. Protein crystallization and phase diagrams. *Methods* **2004**, *34*, 266–272. [[CrossRef](#)] [[PubMed](#)]
15. Luft, J.R.; DeTitta, G.T. A method to produce microseed stock for use in the crystallization of biological macromolecules. *Acta Crystallogr. D Biol. Crystallogr.* **1999**, *55*, 988–993. [[CrossRef](#)] [[PubMed](#)]
16. Oksanen, E.; Chen, J.C.; Fisher, S.Z. Neutron crystallography for the study of hydrogen bonds in macromolecules. *Molecules* **2017**, *22*, 596. [[CrossRef](#)] [[PubMed](#)]
17. Fisher, Z.; Jackson, A.; Kovalevsky, A.; Oksanen, E.; Wacklin, H. Biological structures. In *Experimental Methods in the Physical Sciences*; Felix, F.-A., David, L.P., Eds.; Elsevier: San Diego, CA, USA, 2017; Volume 49, pp. 1–75.
18. Blum, M.-M.; Tomanicek, S.J.; John, H.; Hanson, B.L.; Rüterjans, H.; Schoenborn, B.P.; Langan, P.; Chen, J.C.-H. X-ray structure of perdeuterated diisopropyl fluorophosphatase (DFPase): Perdeuteration of proteins for neutron diffraction. *Acta Crystallogr. F Struct. Biol. Cryst.* **2010**, *66*, 379–385. [[CrossRef](#)] [[PubMed](#)]
19. Tanaka, I.; Kusaka, K.; Hosoya, T.; Niimura, N.; Ohhara, T.; Kurihara, K.; Yamada, T.; Ohnishi, Y.; Tomoyori, K.; Yokoyama, T. Neutron structure analysis using the IBARAKI biological crystal diffractometer (iBIX) at J-PARC. *Acta Crystallogr. D Struct. Biol.* **2010**, *66*, 1194–1197. [[CrossRef](#)] [[PubMed](#)]
20. Pastorek, J.; Pastorekova, S. Hypoxia-induced carbonic anhydrase IX as a target for cancer therapy: From biology to clinical use. *Semin. Cancer Biol.* **2015**, *31*, 52–64. [[CrossRef](#)] [[PubMed](#)]
21. Alterio, V.; Hilvo, M.; Di Fiore, A.; Supuran, C.T.; Pan, P.; Parkkila, S.; Scaloni, A.; Pastorek, J.; Pastorekova, S.; Pedone, C.; et al. Crystal structure of the catalytic domain of the tumor-associated human carbonic anhydrase IX. *Proc. Natl. Acad. Sci. USA* **2009**, *106*, 16233–16238. [[CrossRef](#)] [[PubMed](#)]
22. Kazokaite, J.; Niemans, R.; Dudutiene, V.; Becker, H.M.; Leitans, J.; Zubriene, A.; Baranauskiene, L.; Gondi, G.; Zeidler, R.; Matuliene, J.; et al. Novel fluorinated carbonic anhydrase IX inhibitors reduce hypoxia-induced acidification and clonogenic survival of cancer cells. *Oncotarget* **2018**, *9*, 26800–26816. [[CrossRef](#)] [[PubMed](#)]
23. Mahon, B.P.; Bhatt, A.; Socorro, L.; Driscoll, J.M.; Okoh, C.; Lomelino, C.L.; Mboge, M.Y.; Kurian, J.J.; Tu, C.; Agbandje-McKenna, M.; et al. The Structure of Carbonic Anhydrase IX Is Adapted for Low-pH Catalysis. *Biochemistry* **2016**, *55*, 4642–4653. [[CrossRef](#)] [[PubMed](#)]
24. Ireton, G.C.; Stoddard, B.L. Microseed matrix screening to improve crystals of yeast cytosine deaminase. *Acta Crystallogr. D Struct. Biol.* **2004**, *60*, 801. [[CrossRef](#)]
25. Koruza, K.; Lafumat, B.; Végvári, Á.; Knecht, W.; Fisher, S.Z. Deuteration of human carbonic anhydrase for neutron crystallography: Cell culture media, protein thermostability, and crystallization behavior. *Arch. Biochem. Biophys.* **2018**, *645*, 26–33. [[CrossRef](#)] [[PubMed](#)]
26. Budayova-Spano, M.; Fisher, S.Z.; Dauvergne, M.-T.; Agbandje-McKenna, M.; Silverman, D.N.; Myles, D.A.A.; McKenna, R. Production and X-ray crystallographic analysis of fully deuterated human carbonic anhydrase II. *Acta Crystallogr. F Struct. Biol. Cryst. Commun.* **2006**, *62*, 6–9. [[CrossRef](#)] [[PubMed](#)]
27. Di Costanzo, L.; Moulin, M.; Haertlein, M.; Meilleur, F.; Christianson, D.W. Expression, purification, assay, and crystal structure of perdeuterated human arginase I. *Arch. Biochem. Biophys.* **2007**, *465*, 82–89. [[CrossRef](#)] [[PubMed](#)]

